Analyzing of in-cylinder flow structures and cyclic variations of partially premixed combustion in a light duty engine

F2016-ESYF-005

ANALYZING OF IN-CYLINDER FLOW STRUCTURES AND CYCLIC VARIATIONS OF PARTIALLY PREMIXED COMBUSTION IN A LIGHT DUTY ENGINE

[1]Tanov, Slavey*; [1]Johansson, Bengt; [2]Izadi Najafabadi, Mohammad; [3]Wang, Hua
[1] Division of Combustion Engines; Lund University; Sweden
[2] Division of Combustion Technology; Eindhoven University of Technology; Netherlands
[3] Dantec Dynamics; Denmark

KEYWORDS – Partially premixed combustion, multiple injection strategies, high-speed particle image velocimetry, proper orthogonal decomposition, cycle to cycle variation

ABSTRACT

Partially Premixed Combustion (PPC) strategy offers the potential for simultaneously reduction of NOx and soot emissions with high efficiency. This low temperature combustion strategy involves a proper mixing of fuel and air prior to auto-ignition. During ignition delay (ID) the exact amount of premixing is crucial for the combustion behaviour and emission formation.

In this article, high-speed particle image velocimetry (HS-PIV) has been applied to characterise the in-cylinder flow and cycle-to-cycle variations in a light-duty optical engine during fired conditions. The engine is operated at 800 rpm and at a constant CA 50 (~ 8 CAD aTDC). Multiple injections strategies (single, double and triple injections) have been applied to investigate their influence on the flow inside the piston bowl and squish region. The 2D velocity fields are evaluated and investigated over a range of crank angles in the compression and expansion strokes in order to understand the cycle-to-cycle variations. To investigate the problem of cyclic- variations on in-cylinder flows the phase-invariant proper orthogonal decomposition (POD) technique was used. The POD decomposition technique provides a classification method based on an energy criterion by which the mean flow is seen as a superposition of coherent structures. From their temporal coefficients it is possible to characterize its dynamical behaviour.

INTRODUCTION

Simultaneous reduction of nitric oxides (NOx) and soot emissions is a tough challenge to conventional Diesel engine even though it possesses higher brake thermal efficiency as compared to spark ignition (SI) engines. Achieving higher brake thermal efficiency along with low levels of emissions is a practical challenge to existing engines. Today, partially premix combustion (PPC) is one of many other low temperature combustion (LTC) system/concepts which can reduce both NOx and smoke emissions simultaneously to very low level without using any after treatment devices along with comparable brake thermal efficiency to conventional CI engines.

PPC is well known as a hybrid combustion concept between HCCI and diffusion combustion (1,2,3,4). In PPC the fuel and air are not fully mixed. The benefit of this concept compared to traditional HCCI combustion is that the final fuel injection can be used as control parameter for the combustion phasing. It involves a certain amount of premixing of fuel air before auto-ignition. The premixing of the mixture inside the cylinder is important for combustion behavior and emission formation. Therefore, PPC is much easier in the gasoline auto-ignition range (RON > 60, CN < 30) because the higher ignition delay allows more time for mixing of the fuel and oxygen before combustion starts (5). This mixing process in Light-Duty (LD) engines is mainly dominated by the fuel injection process and the strong air motion in the cylinder. The interactions of swirling flow, injected fuel spray, deflection at the combustion chamber walls and entrainment results in energetic rotating flow structures in the piston, which plays an important role in the mixture-preparation process and the late-cycle mixing process (6, 7, 8). Therefore, an understanding of the in-cylinder flow field is crucial to identify the sources of pollutant species in automotive Diesel engines. It is also essential to have in-cylinder flow field measurements to validate numerical modelling efforts, as the ability to quantitatively predict these structures is necessary for engine design using computer-based optimization.

In order to investigate the complex in-cylinder motion and cycle variations, particle image velocimetry (PIV) as a non-intrusive laser diagnostic has already proven its applicability as a useful tool in engine diagnostics. The combustion in spark ignition (SI) engines is influenced by the large scale tumbling flow and is also very vulnerable to cyle-to-cyle variations. Due to the insufficient space as the piston is moving upward at the late phase of compression stroke, the organized, large-scale motion breaks up into small-scale turbulence. In this way, the turbulence intensity is amplified. However, as many researchers have pointed out, this in-cylinder flow process causes large cyclic variations (9,10). Other studies from Muller *et al*. (11), Peterson and Sick *et al*. (12), Krishna and Mallikarjuna *et al* (13) showed the applicability of high speed particle image velocimetry (HSPIV) near the spark plug region in SI engines. Deslandes et al. (14, 15) characterized the swirl and squish evolution in a transparent Diesel engine through a combined PIV and proper orthogonal decomposition (POD) analysis.

More earlier experimental studies on engine flows using PIV have been focused on showing the cycle-to-cycle variations of the mean flow, Reuss *et al*. (16,17), Mouqallid *et al*. (18), Trigui *et al*. (19). The results showed that the ensemble mean flow was not representative for the instantaneous velocity maps. Only when cycle-by-cycle averaging (low-pass filtering) was used it was possible to obtain better approximations of the instantaneous velocity flow field. Regarding the PIV measurement under LTC conditions, Hildingsson and Miles *et al.* (20). measured vertical plane velocity fields which describes the bulk flow structures in a LD Diesel engine with re-entrant optical piston bowl shape to evaluated the fuel air mixture and the production of emissions (21). Tanov and Zhenkan *et al*. (22,23) presented the influence of multiple injection strategies on in-cylinder fluid motion under motored and fired cycles with a typical production piston with re-entrant bowl shape. They highlight that the turbulence is highly depended on the last fuel injection before TDC. First and/or second injections showed limited effect on turbulence.

In such situations, flow decomposition methods like POD and dynamical mode decomposition (DMD) can be extremely powerful tools for the analysis of such complex flows, since they give a basis for an objective quantification of the relative magnitude of the observed flow phenomena and their spatial structure (24).

POD is a mathematical technique used to obtain low dimensional approximate descriptions of high-dimensional processes or to extract main modes from experimental data. Druault *et al.* (25) used POD to determine flow information between two consecutive PIV flow images. Roudnitzky *et al.* (26) used the POD technique to PIV measurements obtained in the tumble plane of spark ignition engine flow. In this study, the in-cylinder flow was decomposed into an average part, a coherent part and a random Gaussian fluctuations part. Fogleman *et al.* (27) introduced a novel approach called phase-invariant POD on both computational fluid dynamics (CFD) and PIV data. The phase-invariant POD modes were desirable to provide a suitable basis for low-dimensional models, which would describe the breakdown process of tumble. Kapitza *et al.* (28) utilized POD to investigate the role of the intake port flow on in-cylinder flow fluctuations. Vosine *et al.* (29) also used POD to investigate in-cylinder flow structures and their CCV. POD has also been used as an objective means for comparing PIV results and data from large eddy simulations (30, 31).

Up to now, a large number of systematic studies have reveled in-cylinder flow studies in SI engines and compressions ignition (CI) engines utilizing a conventional combustion. However, relatively little work has been reported on the influence of injection strategies under PPC condition, especially for gasoline fuel PPC combustion. The results in the first part demonstrate the ensemble average vector fields in the clearance volume and bowl region. Vertical-plane velocity measurements are obtained with a HSPIV technique in an operating direct-injection Diesel engine with fuel injection and its associated heat release. Furthermore, the second part of results presents the cycle to cycle variation studies by using POD method. The POD decomposition technique provides a classification method based on an energy criterion by which the mean flow is seen as a superposition of coherent structures. From their temporal coefficients it is possible to characterize its dynamical behavior and quantity the cyclic variability.

EXPERIMENTAL APARATUS

The measurements were performed in an optical LD direct-injection Diesel engine at the Combustion Engine Department of Lund University. A five-cylinder research engine was modified from a Volvo V5 production engine that has a displacement of 480 cm^3 per cylinder. The engine was converted to single-cylinder operation with a Bowditch piston extension. The remaining four pistons were motored and equipped with counter weights to compensate for the extra weight of the piston elongation. The main geometric characteristics are summarized in Table 1, followed by a schematic view of the optical engine (Figure 1). Additionally, a full quartz liner in the upper cylinder part and a full quartz piston-top permit optical access into the combustion bowl from the side. The quartz piston retains a realistic bowl geometry in order to maintain the in-cylinder flow as similarly as possible to the flow that would exist in a production engine. The engine further allows the intake swirl to be adjusted by a swirl control valve. A maximum swirl ratio of 2.6 is employed for the measurements reported here. For fuel injection, the engine is equipped with a Bosch common rail fuel-injection system.

During the recording of all combustion events, the cylinder pressure was simultaneously recorded at every 0.2 CA. The experimental heat release rate was computed from the cylinder pressure data using the first law analysis. Heat transfer was estimated by using the Woschni equation (32).

Engine base type	Volvo D5
Number of cylinders	5
Number of valves	4
Bore	81 mm
Stroke	92.3 mm
Connecting rod	147 mm
Displacement	0.48 L
Compression ratio (metal configuration)	1:16
Compression ratio (optical configuration)	1:11.3
Swirl ratio	2.6
Fuel Injection	
Type	Common Rail
Fuel-injector type	Solenoid
Hydraulic flow	360 cc/30s @ 100 bar
Umbrella angle	140°
Orifice diameter	0.159 mm
Number of holes	5
Hole conicity	1.5

Table 1: Engine geometric properties

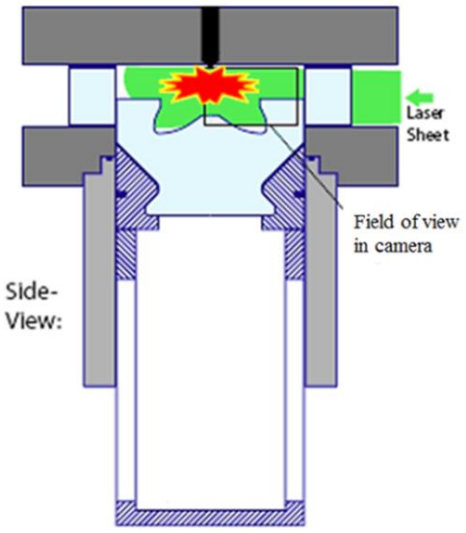

Figure 1: Schematic of the optical engine and the experimental configuration.

PIV MEASUREMENT SYSTEM

An Nd: YLF diode pumped dual cavity laser from Dantec Dynamics (model type: DualPower 30-1000), was used here as the light source. Its wavelength is 527nm and can reach maximum 30mJ power per pulse at a running repetition rate 1 kHz. In the case of engine running at 800rpm, the laser shoots at 2.4kHz, with 13mJ energy per pulse. A light sheet optics unit was used to generate a diverging light sheet. The light sheet was passing through the injector tip, and focused in the area between injector tip and liner inner surface in the thickness-wise view. The light sheet had a height around 3 cm through the field of view.

Titanium Dioxide (TiO2) powder was used as PIV seed particles, which have a mean particle diameter from 2 to 3 um and a density of 4260 kg/m3. Assuming Stokes drag, the particle time constant (τs) – representing the response time to changes in the flow – is roughly 40 us at TDC-like thermodynamic conditions. At these conditions, τs is slightly larger than the estimated Kolmogorov time scale and thus the seeding particles should follow most of the turbulent structures. Seeding particles were introduced from a cylindrical container fed by a swirl airflow of around 20 liters/min, which was precisely controlled by a mass flow meter. The seeding flow was then mixed with the intake stream inside the intake manifold. The TiO2 powder was baked over 24 hours before seeding into the engine, to prevent the particles agglomeration efficiently. In addition, water vapor was added to the intake stream, as part of EGR gases, to reduce the electrostatic charge build-up, and eventually to reduce the chance of

having the particles adhere to the optics of the engine. These two procedures were proved to be essential for engine in-cylinder PIV measurement.

Images were acquired using a Dantec Dynamics high speed CMOS camera (SpeedSense 710). The image format was cropped to 1040*440 to increase the max. camera frame rate. The exposure time for all image pairs was 63 μs for the first image and around 350 μs for the second image (depends on the engine rotation speed). The long exposure for the second image was due to the time required to readout the first image from camera sensor. The time between the laser pulses was set to 15 μs, which is a good compromise between resolving velocity and being able to perform the cross-correlation. A synchronization system was used to synchronize both camera exposure and laser to engine rotation so one image pair can be obtained every crank angle degree.

No filter was used in this measurement, since it was proved that there was little soot luminosity from PPC combustion thus the Mie scattering light from particles was dominant here.

The optical piston with a similar bowl geometry with a realistic one would bring significant optical distortion to the acquired image. Considering the piston glass has irregular thickness in the optical path and the distortion might depend on the piston position with respect to the camera lens, this distortion is almost impossible to be compensated by adding additional optics between the engine and the camera; and so far it can be only handled by software image dewarping. A Nikkor 105 mm lens with an extension ring (Nikkor PK-13) was used here and the lens aperture was closed as much as possible (f# 16) to obtain focus in the full field of view. Together with the used camera, the resulted spatial resolution is aournd 25μm/pixel.

OPERATING CONDITIONS

In this study, engine measurements were carried out at an engine speed of 800 rpm and an injection pressure of 850 bar for three different injection strategies (single, double, triple injection). Combustion phasing (CA50) was kept constant at around 8 CA aTDC. At SOC the fuel/air mixture is stratified to achieve stable ignition and controlled heat release. The inlet air temperature was 40 °C and the intake air pressure was 1.2 bar. The experiments were performed in a randomized order after the engine reached a steady thermal state that corresponded to a cooling water temperature of 65 °C. The operating conditions are summarized in Table 2 and the rates for heat release and pressure are computed in Figure 2. Multiple injections were used in order to achieve less fuel stratification due to more premixing of fuel. As presented in (32) double and triple injection cases demonstrate less fuel stratification. The premixing is promoted using PRF70 and early fuel injections in the compression stroke in order to increase the ignition delay prior auto-ignition. It can be seen from Figure 2 that maximum heat release rate can indeed be reduced by using multiple injections.

Engine parameters			
Intake pressure		1.2 bar	
Intake temperature		40 °C,	
Injection pressure		850 bar ±2 bar	
Fuel mass per injection		~12.4 mg	
Swirl ratio		2.6	
O_2		21 vol%	
Skip fire sequence		1:5	
Cooling water temperature		65 °C ± 2 °C	
Liner wall temperature		80 °C	
Fuel type		PRF 70	
Seeding		TiO_2	
Injection timing		SOI [CAD]	Duration [CAD]
Case A	Single	16	2.5
Case B	Double	40/16	1.9/2
Case C	Triple	55/30/18.5	1.7/1.7/2

Table 2: Operating conditions

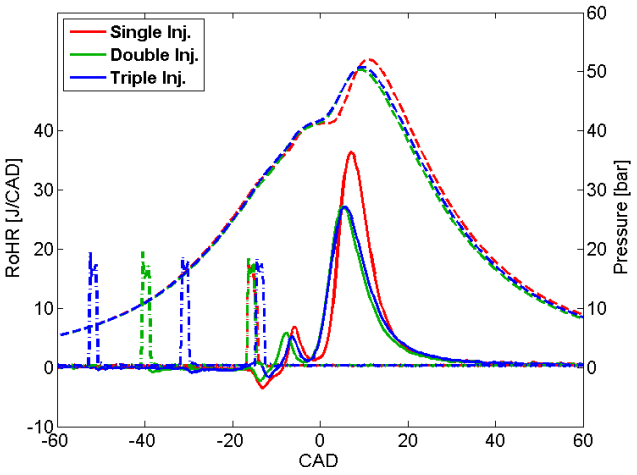

Figure 2 Pressure an heat release rates at constant combustion phasing (CA50 = 8 CA aTDC)

IMAGE DEWARPING

As mentioned in the previous section, the images were severely distorted as a result of the irregular geometry of the optical piston bowl. An image distortion correction programme was developed using MATLAB. To allow for software image distortion, a pair of calibration target images must be acquired, both with and without distortion. The calibration target is made from paper (with a thickness of 1 mm to avoid bending while it is inserted into the piston) that is marked with dots having uniform 1 mm × 1 mm spacing on its surface. The paper has the same geometry as the piston bowl. As shown in Figure 3(a), the dot spacing was fairly uniform in the radial direction but varied significantly in the axial direction.

The image dewarping programme was developed to select an individual corresponding dot from the undistorted and distorted images, respectively, and then test a number of transformation routines in order to determine the best fit for the final transformed image. In the end, a “local weighted mean” transformation—in which a separate linear transformation is applied locally—provided the best image correction for the images. Previously, other research groups used “piecewise-linear transformation” (21), which is similar to the method used in this study; however, that model is more demanding to the dots’ location and spacing, and was not successfully implemented in this study. Figure 3(a) and 3(b) shows a dot target (customized for this piston bowl) image before and after applied the image dewarping. As shown in Figure 3 (b), most of the dots are clearly seen and uniformly spaced. Unfortunately, the bottom of the piston bowl gives most severe distortion and couldn’t be handled by this measurement.

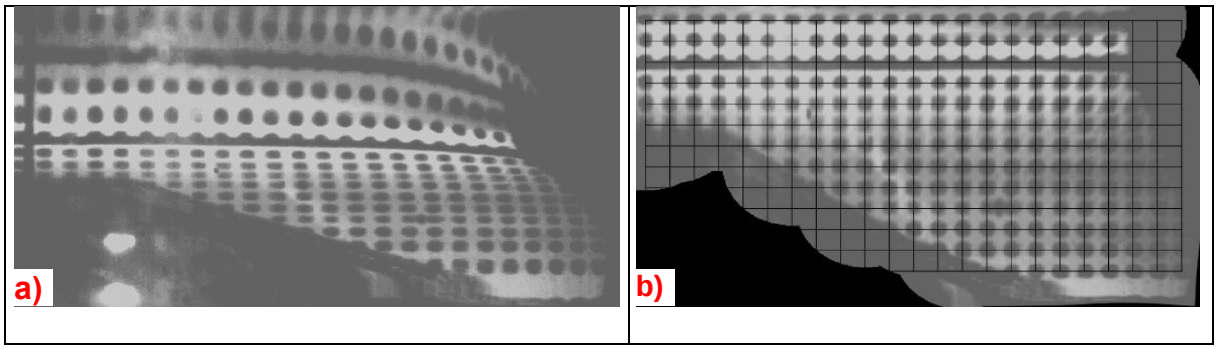

Figure 3: Target image: before distortion correction (a) and after distortion correction (b).

PIV VECTOR EVALUATION

Velocity vectors were computed on the dewarped image pairs using Adaptive PIV, a commercial PIV processing software provided by Dantec Dynamics. This method allows the interrogation area (IA)—based on which the cross correlation is computed—to iteratively adapt its size, shape, as well as orientation in order to improve the calculated vector accuracy in the end. With this method, the processed vector field is not sensitive to the input of IA size—as long as the input is in a reasonable range. In this study, the IA size was selected to start with 64 × 32; it can go down to 16 × 8 during iteration, giving it a fairly large range. Once the raw vector maps had been computed, a moving average algorithm was first applied to the raw individual field to remove outline vectors. The filter size was 5 × 5 vectors. With this method, each vector was replaced by the median value of the surrounding eight neighbours.

The ensemble average analysis is based on flow registrations divided into a number of time slots to resolve the largest flow structure. In this study, about 40 consecutive cycles were conducted to obtain PIV measurement data. Hence, the ensemble average analysis was calculated based on every two CA. The definition of ensemble average is:

$$\overline{U}_{EA}(\theta) = \frac{1}{N}\sum_{i=1}^{N} U(\theta, i) \qquad (1)$$

Where U is instantaneous velocity, θ indicates the CA, i is the cycle index, and N is the number of cycles.

ANALYSIS METHODS

POD, is closely related to Principal Component Analysis, PCA, from linear algebra and was first introduced in the context of Fluid Mechanics by Lumley (33). This implementation of POD applies the so-called "Snapshot POD" proposed by Sirovich (34). Each instantaneous PIV measurement is considered a snapshot of the flow. An analysis is then performed on a series of snapshots acquired in the same position and under identical experimental conditions. The first step is to calculate the mean velocity field from all the snapshots. The mean velocity field is considered the zero'th mode of the POD. Subtracting the mean from all snapshots, the rest of the analysis operates on the fluctuating parts of the velocity components (u_{mn}, v_{mn}) where u & v denote the fluctuating part of each velocity component. Index m runs through the M positions (and components) of velocity vectors in each snapshot and index n runs through

the N snapshots so u_{mn}= u (x_m,y_m,t_n). All fluctuating velocity components from the N snapshots are arranged in a matrix U such that each column contain all data from a specific snapshot:

$$U = \begin{bmatrix} u_{11} & u_{12} & \cdots & u_{1N} \\ \vdots & \vdots & \vdots & \vdots \\ u_{M1} & u_{M2} & \cdots & u_{MN} \\ \hline v_{11} & v_{12} & \cdots & v_{1N} \\ \vdots & \vdots & \vdots & \vdots \\ v_{M1} & v_{M2} & \cdots & v_{MN} \\ w_{11} & w_{12} & \cdots & w_{1N} \\ \vdots & \vdots & \vdots & \vdots \\ w_{M1} & w_{M2} & \cdots & w_{MN} \end{bmatrix} \leftarrow \begin{cases} \text{Time series of a specific velocity} \\ \text{component in a specific point} \end{cases}$$

$$\overbrace{\qquad\qquad}$$

Snapshot = All velocity components in all points at a specific point in time

(2)

Using the velocity matrix, the N 9 N space correlation matrix, or autocovariance matrix, is defined as:

$$R = \mathbf{U}^{\mathrm{T}}\mathbf{U} \tag{3}$$

for which the eigenvalue problem can be written as

$$RA = \Lambda A \tag{4}$$

-where λ and A(i) are corresponding eigenvalues and -vectors. Solutions are ordered according to the size of their eigenvalues:

$$\lambda_1 > \lambda_2 > \ldots > \lambda \tag{5}$$

Since the subtracted mean value was calculated from the data itself the N'th eigenvalue will always be zero and can in practice be discarded. The eigenvectors (A) are sorted in the same order as the eigenvalues and stored as a matrix used to define the POD mode matrix (U) which is normalized:

$$\Phi = \frac{A\mathbf{U}}{\|A\mathbf{U}\|} \tag{6}$$

The POD coefficients (a_i) for a specific snapshot are determined by projecting the velocity field of the snapshot onto the POD modes:

$$a_i^n = \Phi^i U^n \tag{7}$$

Using the POD coefficients and the POD modes, a snapshot (n) can be reconstructed using:

$$U_r^n = \sum_{i=1}^{i_{max}} a_i^n \Phi^i \tag{8}$$

When all POD mode contributions are included (i_{max} = N), the snapshot is fully reconstructed.

RESULTS AND DISCUSSION

Single injection

The evolution of the flow field for the single injection case from -45 CA to 25CA is shown in Figure 4. At-45 CA, the flow field is directed upwards, according to the ascending piston

motion. As the piston continues to move up, the flow directly above the bowl lip begins to deflect towards the center of the bowl at -35 CA. Moreover, a noticeable occurrence in the vertical vector plane, close to the optical liner, shows a consistently behavior of the flow with a radial direction from -45 CA to -25 CA. This is most likely due to the impact of the angular momentum from the inlet and swirl ports.
As the piston enters the field of view at -30 CA, it is interesting to note that the direction of the squish flow has changed and efforts to penetrate in to the bowl. The degree of inward penetration of the squish flow is thus primarily determined by a competition between the radial momentum imparted to a fluid element during the squish process, and the increasing centrifugal forces acting on the element as it penetrates inward. Centrifugal forces will clearly be dependent on the flow swirl level, and less penetration is noticeable at the highest swirl levels of this engine configuration(R_s=2.6) (20). Since PIV measurement in a curved piston are very complex some area of the piston couldn't be illuminated by the laser. As a results of this weakness, these areas are white and does not consist any vectors. We therefore determine based on the velocity vectors in the clearance volume that flow begins to enter the bowl (-25 CA) and stagnation plane is located in the unirradiated white area. In this area two flows are impinging at the stagnation plane, and the incoming squish flow is demanding to push down the flow in the bowl.

Furthermore, without fuel injection, the flow structures in the bowl are primarily generated by piston motion. After fuel is injected, the flow pattern changes due to the associated displacement of the small seeding particles. For the single injection case the fuel is directed into the bowl, just below the lip (-15 CA). Interactions of the jets with the bowl wall result in the formation of a strong, clockwise-rotating vertical structure within the bowl with velocities around 7–8 m/s. However, this vortex is a result of both spray-induced motion and squish flow, resulting in a stronger flow structure and is clearly visible till TDC with relocation of its centre point. By +5 CA the vortex structure starts to break down due to combustion event and ascending piston motion an intense upward and downward fluid motion during heat release (10 CA,15 CA) was observed. Furthermore, at +15 CA at the location of the piston lip a reverse squish flow appears due to the rapid heat release. The location of heat release can be directed from the flow field by identifying the volumetric source of the expanding flow structure. In each of this CA's there seem to be more than one sources of volumetric expansion. Nevertheless, the flow development in the piston during the expansion between 20 and 35 CA is similar. For the same CA's the flow pattern in the clearance volume is similar as well. A toroidal vortex above the piston begins to take shape. The shape and location of the vortex corresponds to images of soot and partially oxidized fuel (21). Fluid from this region may contribute substantially to unburned hydrocarbon or CO emissions due to the large volume occupied. Beyond 35, the data from the bowl region are no longer available because the region moves out of the measurement area.

Another interesting feature during expansion is the absence of radially flow in the squish volume and near the cylinder centreline. This lack of flow structure near the injector tip to facilitate transport and mixing are preferred zones of CO and UHC emissions. In (37) also the authors show, a fuel vapour cloud forms at 30°CA around the injector tip as the sac volume dribble evaporates.

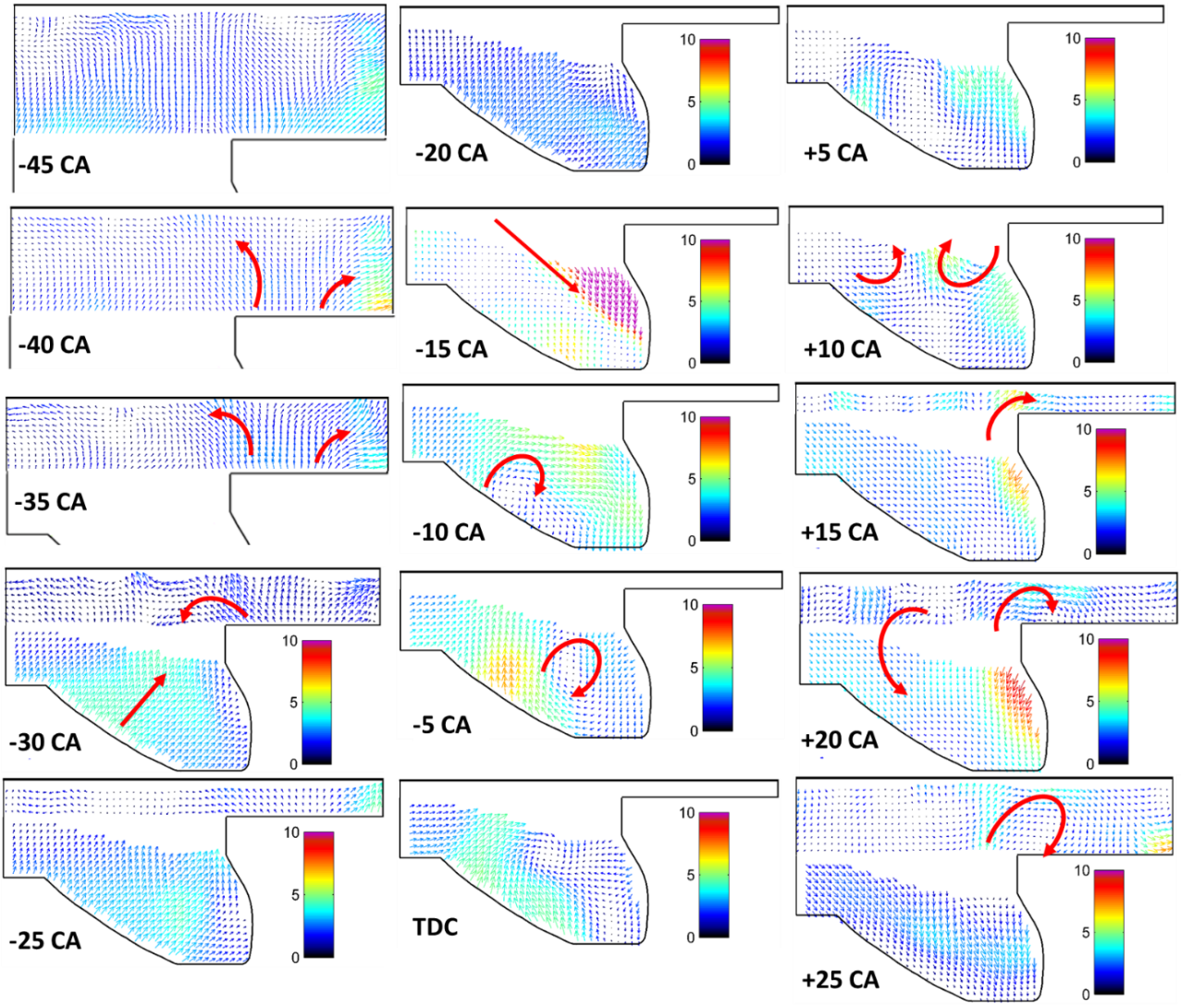

Figure 4: Mean flow field at different CA positions for single injection (Case A: SOI = -16 CA)

Double injection

Figure 5 demonstrate the ensemble average vector fields for double injection case from. The image sequence begins at -45 CAs in order to be able to demonstrate the effect of the first injection. In this case first fuel was injected at -40 CA. The vector field at this CA shows the influence of injection process. This is mainly because the fuel jet itself carries a large amount of flow momentum and kinetic energy, which is transported towards the piston surface. Moreover, at -35 CA it is clearly visible that fluid in the clearance volume is pointing perpendicular on the optical liner. As a result of this flow behaviour, the first fuel injection can lead to an increased UHC and CO emissions in the crevice volume. As the piston continues to move upwards, the clearance volume gets compressed and the fluid flow above the piston lip starts to deflect towards the cylinder centre line. This flow structure is shown from -35 CA till -20 CA. The second injection timing was set to -16 CA. After this at -15 CA, the fuel jet gradually penetrates into the ascending piston bowl. At -5 CA we observed a clockwise rotating vortex like for single injection. This vortex is a result of the deflected spray momentum at the piston bowl wall. Further at TDC, when the fuel and air is sufficient mixed together starts to auto ignite close TDC. Once the combustion starts, the in-cylinder flow

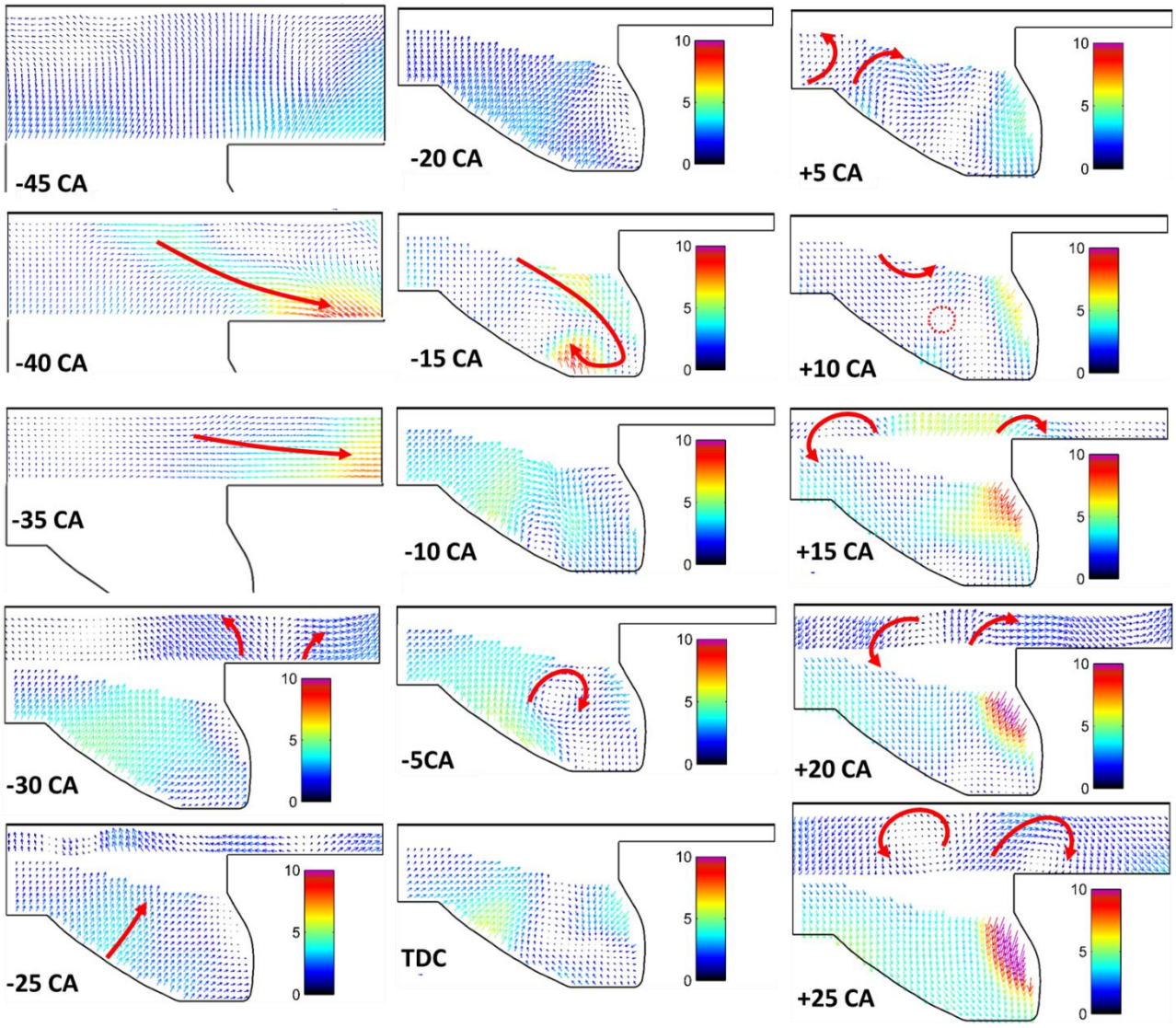

Figure 5: Mean flow field at different CA positions for double injection (Case A: SOI = -40/-16 CA)

changes significant. At TDC the vortex starts to break down and at +5 CA a consistent flow pattern within the piston bowl is hard to observe. Again, like in single injection case, a counter clockwise rotating flow motion at the piston pip region can be observed. AS the HR becomes significant (+10 CA) a strong fluid motion in all direction exists. The gas expansion due to rapid heat release acts to displace the seeding, which further lead to an enhanced flow motion, created low in the bowl. After the peak heartsease, at 15 CA a considerable part of the squish region becomes visible again. At this CA, close to the piston the fluid begins to exit the bowl and enter towards squish region. This reverse squish flow motion strengthens and is further emphasized at +20 CA. Furthermore, the counter clockwise vortex is still present between 15-20 CA and is located just above the bowl opening. The reverse squish motion observed earlier is also present for higher CA, when the flow is expanding downward following the piston motion. At + 35 CA and beyond, the piston has moved out of the vertical measurement plane and data from the bowl are not available. From 40-45 the all over dominating flow direction is downwards together with a looping reverse squish flow due to the expansion caused by the piston motion.

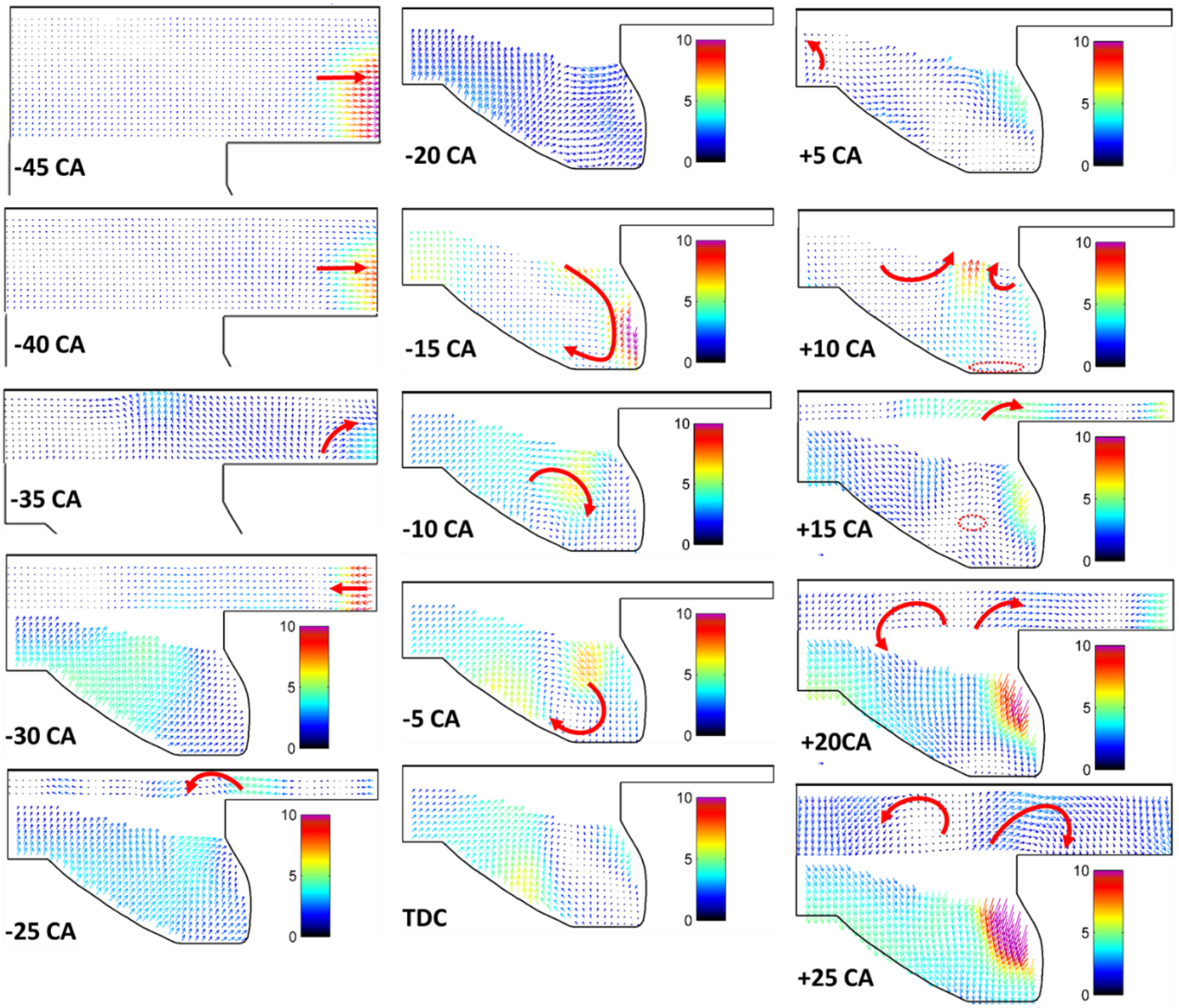

Figure 6: Mean flow field at different CA positions for triple injection (Case A: SOI = -55/-30/-16 CA)

Triple injection

Figure 6 illustrates the flow pattern obtained for the triple injection strategy in which fuel was injected at 55/30/18.5 CA bTDC. The engine cycle starts with a pulse of low reactivity fuel during the compression stroke at -60 CA. This fuel pulse is timed to mix sufficient enough with the intake air prior to hot auto-ignition which occurs further in the piston bowl floor. The fuel is entering the compressed air rapidly with very fast atomization and vaporization in the bulk gas. The flow field at -45 CA differs greatly from single and double injection. As a consequence of the first injection event, a dominated fluid motion towards the optical liner in the clearance volume are observed. Second injection pulse is used to utilize a stratified charge with the fuel from the first injection event. Subsequent to the second fuel pulse, the jet induced motion opposes the squish flow near the liner towards centreline/piston bowl. Furthermore, at -25 CA, the flow field in the squish region gets deflected and shows a tendency to enter the bowl. As a result of this tendency we presume that the injected fuel from the first and second events are mixed together and entering the bowl region. For following CA positions (-20 till +20 CA), the height of squish region is found to be approximately 1 mm and consequently, we could not obtain any fluid motion within the narrow measurement field.

At -20 and -15 flow field in the bowl is principally generated by piston motion. The fuel jet corresponding to the third injection therefore penetrates briefly into the piston, higher on the bowl lip. These conditions result in a shorter ignition delay and is used to trigger the combustion of the premixed fuel/air mixture. Subsequently at -10 and -5 a clockwise vortex appears in the mean field due to a combination of squish flow and spray-induced flow. For TDC position the organized flow pattern starts to change its structure on behalf of start of combustion. The peak HR occurs at +5 CA and an unorganized fluid motion are observed. Combustion is already well established following auto-ignition of the fuel introduced during the injection events leading to an increase in bulk gas temperatures and combustion-induced expansion, which causes velocity fluctuation within the piston bowl. After the heat release (beyond +20 CA), the flow inside the bowl is nominally directed downwards, corresponding to the piston motion. At the later CA positions (beyond +25 CA), the presence of the flow progress in the squish volume is similar what is found in single and double injection case. Fansler and French (36) have delivered a reason for the occurrence of this phenomena. With a re-entrant bowl, fluid beneath the bowl rim must flow inward to pass through the bowl throat as the piston descends. However, the expanding squish volume dictates that the flow be outward at and above the bowl throat. The radial flow must therefore undergo a reversal near the bowl lip, leading to regions of large radial momentum. This effect is absent, or greatly diminished, in non-reentrant bowls, although numerical studies suggest there may be modest reverse-squish turbulence production near the lip for these geometries also (38).

CAYCLIC VARIATION ANALYISIS BY POD

The determination of orthogonal basis functions the cutoff mode M is based on two outstanding properties of the mean part: the large amount of the kinetic energy is distributed to mode M; the flow fields reconstructed by M first dominant modes have a negligible cyclic variability and are highly correlated. These criteria allow to distinguish the mean and fluctuation parts. The method profits from the standard deviation of the POD temporal coefficients permitting a cycle-to-cycle variation evaluation. At a given CA, the standard deviation of the temporal coefficients corresponding to the nth POD mode is calculated.
As discussed above, the POD analysis here described based on the acquisition of several snapshots at a fixed CA over 44 cycles, on which a POD technique is then performed. For better understanding of POD in Figure 7 we show the energy fraction as a function of the mode numbers. In general, we obtain the same number of modes as the snapshot numbers. However, in Figure 7. only 20 modes numbers are utilized due to the fact that the correlation curves are converged to 1% of energy fraction or even less. Each curve corresponds to different CA: case 1 represents the late phase of compression stroke, case 2 during the combustion and case 3 the expansion stroke. First observation from this plot is that the first modes (lowest mode number) contains the highest kinetic energy and for higher mode numbers the curves for case1 and case 3 show a steep decrease compared to the case 2. In principle, this high concentration in the first POD mode indicates a highly organized flow with small cycle-to-cycle variations. In contrast, case 2 captures only 29 % energy fraction in the first mode as a result of the heat release at this CA. This implies that the flow during combustion (case 2) vary considerably from cycle to cycle, and the flow is relatively disorganized. In principle, about 80% kinetic energy is reached by using the first 5 modes for case 1 and case 2, and for case 3 a larger set of modes is required to obtain a good level of similarity with the original field.

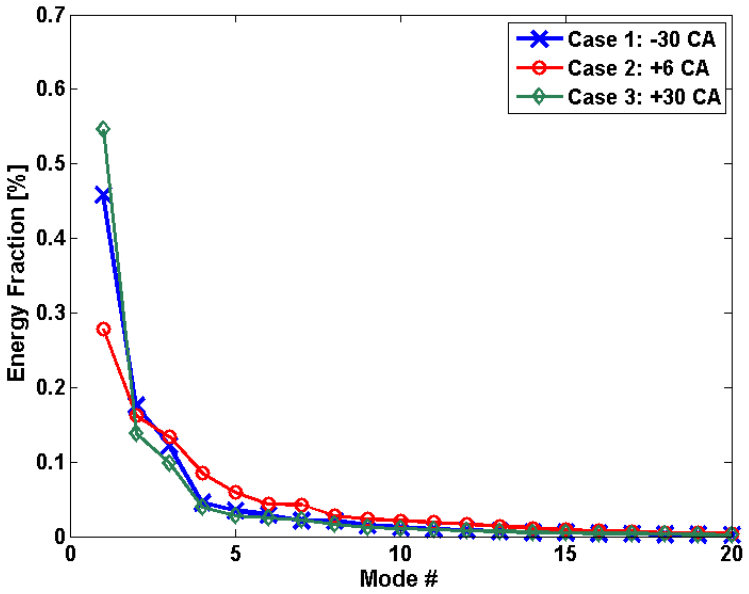

Figure 7: Normalized energy fraction as a function of the POD mode numbers

As discussed earlier, the POD coefficients are obtained by projecting the POD modes onto the original velocity fields. For snapshot POD, this gives a time varying coefficient for each mode. In the case of no cycle-to-cycle variability, the value of a(i) (t) for a particular mode M would be the same at all times that correspond to the same piston position. The magnitude of variation of a(i) (t) at a given piston position for different engine cycles is an indication of cycle-to-cycle variations, and this can be quantified by computing the standard deviation in a(i) (t) at each piston position using by using the first mode.

Figure 8 demonstrate the fluctuation of the POD coefficients at every CA for the temporal resolution from 30 CA bTDC till 30 CA aTDC for single, double and triple injection. The spread in the coefficient values over the 44 engine cycles is greatest around -15 CA and +10 CA. The degree of the spread is quantified by calculating the standard deviation in the coefficient value at each phase. This method is based on the work outlined in (30), a quantitative index for cycle-to-cycle as a function of CA is here derived and computed in Figure 9.

As visible in the graphs, the reported modes present essentially two peaks of fluctuations (Figure 9). The first peak corresponds to the fuel injection. From the PIV data we have obtained an organized flow until the first or last fuel injection. After fuel is injected into the piston bowl, the well-organized flow begins to change and forms a clockwise rotating vortex, causing an increase in the standard deviation of the POD coefficient. Later the in- cylinder flows begin to stabilize prior the mixed fuel and air starts to combust. Following heat release in the combustion chamber, indicating again an increase in the standard deviation of the POD coefficient. This existing second peaks are potential sources of high cycle-to-cycle variations with disorganized flow. For single injection the cycles are varying significantly in contrast to double and triple injection, whereas the combustion induced variations are not significant. After the combustion a coherent flow field appears, and indicates that the coefficients are decreasing during the expansion stroke.

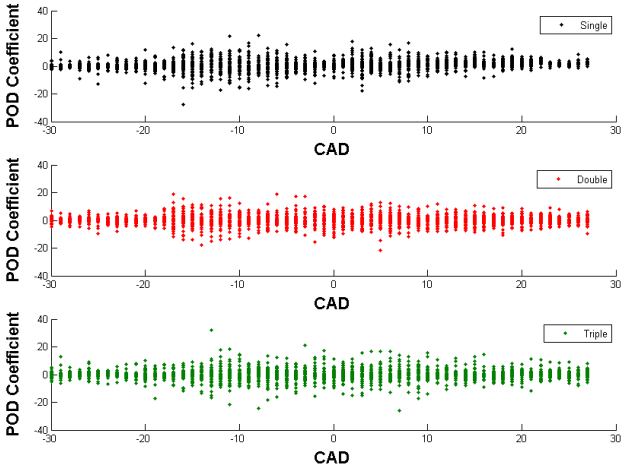

Figure 8: Temporal POD coefficients of mode 1. For each CAD, 44 coefficients illustrate the variation among the 44 cycles.

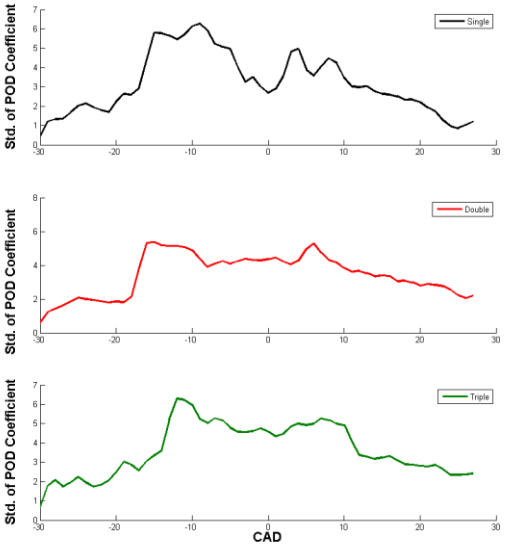

Figure 9: Standard deviation of the coefficients over 44 engine cycles.

SUMMERY AND CONCLUSIONS

This paper provides an approach to simultaneously and quantitatively investigate the in-cylinder conditions and cycle-to-cycle variations during compression and expansion stroke by means of snapshot POD technique. The high-speed PIV experiments were conducted in a single-cylinder optical DI engine by using PPC strategy. The PIV data obtained in the vertical measurement plane provides vector fields from different CAs of 44 consecutive cycles. The mean vector fields are given for the clearance volume and bowl regions for three fired conditions with single, double and triple injection. The following flow features obtained in the measurements clearly define the evolution coherent flow structures within the combustion chamber:

•The squish flow from -45 CA until -30 CA has shown different fluid motions for all cases. For single injection, the flow above the piston lip begins to deflect towards the centerline near -35 CA and also a radial flow on the liner was observed. Additionally, between -30CA a – 25 the flow begins to enter the bowl.

The fluid motion in the clearance volume for double and triple injection have shown strong deviations from single injection case. These deviations are a result of early fuel injections. Double injection demonstrated a strong horizontal fluid flow pointing towards at the liner. In contrast, triple injection case presents the opposite flow motion at -30 CA.

•In all cases, formation of a clockwise rotating vortex in the bowl caused by the injection event occurs from -15 CA until near TDC.

•Once a strong volume expansion occurs, a strong outward and upward fluid motion was observed for each fired condition. Subsequently, this volume expansions indicating location of heat release.

•Beyond +15 CA the flow starts to exit bowl. The fluid close to the piston surface follows the descending movement of the piston. As it moves downward the flow imparts a looping motion to the reverse squish flow and additionally a counter clockwise vortex have formed in the upper part of the bowl (+25 CA).

•POD methodology was applied to the velocity field data with a view to using the approach to evaluate the turbulent structures and cyclic variability within the flow field. In particular, it has been shown that first 5 modes are needed to capture a sufficient amount of total energy. Additionally, there was little change in the lower-order POD modes.

•The magnitude of organized flow varies over the engine cycle and is captured by computing the POD coefficients. Furthermore, the cycle-to-cycle flow variations can be quantified using the standard deviation over engine cycles of the POD coefficients in phase invariant POD analysis.

REFERENCES

[1] Manente V., Johansson B., Tunestal P.," Effects of Different Type of Gasoline Fuels on Heavy Duty Partially Premixed Combustion", SAE 2009-01-2668, 2009

[2] Berntsson A., Denbratt I., "HCCI Combustion Using Charge Stratification for Combustion Control", SAE Technical Paper 2007-01-0210, 2007

[3] Guohong T., Zhi W., Jianxin W., Shijin S., "HCCI Combustion Control by Injection Strategy with Negative Valve Overlap in a GDI Engine", SAE Technical Paper 2006-01-0415, 2006

[4] Miles P. C.," Combined measurements of flow structure, partially oxidized fuel, and soot in a high-speed, direct-injected Diesel engine", Combustion Institute 2963-2970, 2007

[5] Kalghatgi G. "Fuel/Engine Interactions", SAE International, 2006

[6] Miles P., Megerle M., Sick V., Richards K., "The Evolution of Flow Structures and Turbulence in a Fired HSDI Diesel Engine," SAE Technical Paper 2001-01-3501, 2001

[7] Miles P., Megerle M., Hammer J., Nagel Z., "Late-Cycle Turbulence Generation in Swirl-Supported, Direct-Injection Diesel Engines," SAE Technical Paper 2002-01-0891, 2002

[8] Miles P., Megerle M., Nagel Z., Reitz R., "An Experimental Assessment of Turbulence Production, Reynolds Stress and Length Scale (Dissipation) Modeling in a Swirl-Supported DI Diesel Engine," SAE Technical Paper 2003-01-1072, 2003

[9] Frieden D., Sick V., "Investigation of the Fuel Injection, Mixing and Combustion Processes in an SIDI Engine using Quasi-3D LIF Imaging," SAE Technical Paper 2003-01-0068, 2003

[10] Funk C., Sick V., Reuss D., Dahm W., "Turbulence Properties of High and Low Swirl In-Cylinder Flows," SAE Technical Paper 2002-01-2841, 2002

[11] Muller S., Bohm B., Gleißner M., Grzeszik R., Arndt S., Dreizler A.,"Flow field measurements in an optically accessible, direct-injection spray-guided internal combustion engine using high-speed PIV" Exp Fluids 48:281–290,2003

[12] Peterson B., Sick V. "Simultaneous flow field and fuel concentration imaging at 4.8 kHz in an operating engine", Appl Phys B 97:887–895,2009

[13] Krishna B.M., Mallikarjuna J.M.,"Comparative study of incylinder tumble flows in an internal combustion engine using different piston shapes an insight using particle image velocimetry", Exp Fluids 48:863–874,2010

[14] Deslandes W., Dupont A., Baby X., Charnay G., "PIV Measurements of Internal Aerodynamic of Diesel Combustion Chamber," SAE Technical Paper 2003-01-3083, 2003

[15] Deslandes W., Dumont P., Dupont A., Baby X., “Airflow Cyclic Variations Analysis in Diesel Combustion Chamber by PIV Measurements,” SAE Technical Paper 2004-01-1410, 2004
[16] Reuss D.L., Rosalik M., “PIV Measurements During Combustion in a Reciprocating Internal Combustion Engine”, Proc. of the 9th Int. Symp. on App. of Laser Tech. To Fluid Mech., 1998
[17] Reuss D.L., Rosalik M., “PIV Requirements for IC Engine Flows with Large Cyclic Variability”, Proc. of the PIV’99 Symposium,1999
[18] Mouqallid M., Belghit A., Trinite M.,” Application of Cross Correlation Particle Image Velocimetry to the Charaterization of Unsteady Rotating Flow”, Proc. of the 9th Int. Symp. on App. of Laser Tech. To Fluid Mech., 1998
[19] Trigui N., Choi W.-C., Guezennec Y.G., “Cycle Resolved Turbulence Intensity mesurement in IC egines”, SAE Technical Paper Series 962085,1996
[20] Hildingsson L., Hultqvist A., Miles P., “The effect of swirl and injection phasing on flow structures and mixing in an HSDI Diesel engine,” THIESEL, 2006
[21] Miles P., Collin R., Hildingsson L., Hultquist A., Andersson Ö., “Combined measurements of flow structure, partially oxidized fuel, and soot in a high-speed, direct-injection Diesel engine”, Proceedings of the Combustion Institute, 2007
[22] Tanov S., Wang Z., Wang H., Richter M., "Effects of Injection Strategies on Fluid Flow and Turbulence in Partially Premixed Combustion (PPC) in a Light Duty Engine," SAE Technical Paper 2015-24-2455, 2015
[23] Wang Z., Tanov S., Wang H., Richter M., "High-Speed Particle Image Velocimetry Measurement of Partially Premixed Combustion (PPC) in a Light Duty Engine for Different Injection Strategies", SAE Technical Paper 2015-24-2454, 2015
[24] Sanghi S., Hasan N., “Proper orthogonal decomposition and its applications”, Asia-Pac. J. Chem. Eng. 6,2011
[25] Druault P., Guibert P., Alizon F.,” Use of proper orthogonal decomposition for time interpolation from PIV data: application to the cycle-to-cycle variation analysis of in-cylinder engine flows”, Exp. Fluids,2005
[26] Roudnitzky S., Druault P., Guibert P., “Proper orthogonal decomposition of in-cylinder engine flow into mean component, coherent structures and random Gaussian fluctuation”, J. Turbul, 2006
[27] Fogleman M., Lumley J. L., Rempfer D., Haworth D., “Application of the proper orthogonal decomposition to datasets of internal combustion engine flows”, J. Turbul., 2004
[28] Kapitza L., Imberdis O., Bensler H. P., Willand J., Thevenin D., “An experimental analysis of the turbulent structures generated by the intake port of a DISI-engine”, Exp. Fluids, 2010
[29] Voisine M., Thomas L., Boree J. Rey P., “Spatio-temporal structure and cycle to cycle variations of an in-cylinder tumbling flow”, Exp. Fluids, 2011
[30] Liu K., Haworth D., “Development and assessment of POD for analysis of turbulent flow in piston engines”, SAE Technical Paper 2011-01-0830
[31] Sick V., Reuss D., Rutland C., Haworth D., “A common engine platform for engine LES development and validation”, Int. Conf. on LES for Internal Combustion Engine Flows, 2011
[32] Heywood J. B., “Internal Combustion Engine Fundamentals”, McGraw-Hill, Inc., 1988
[33] Lumley J. L., "The structure of inhomogeneous turbulent flow", Atmospheric Turbulence and Radio Wave Propagation, 1967
[34] Sirovich L., "Turbulence and the dynamics of coherent structures. Part I: Coherent structures", Quart. Appl. Math, 1987

[35] Fansler T.D., French D.T., “Swirl, squish and turbulence in stratified-charge engines: laser velocimetry measurements and implications for combustion”, SAE technical paper 870371, Society of Automotive Engineers, 1987
[36] Kim D., Ekoto I., Colban W. F., Miles P. C., "In-cylinder CO and UHC Imaging in a Light-Duty Diesel Engine during PPCI Low-Temperature Combustion", SAE Int. J. Fuels Lubr., 2008
[37] Arcoumanis C., Begleris P., Gosman A.D., Whitelaw J.H., “Measurements and calculationsof the flow in a research Diesel engine”, SAE technical paper 861563, 1986

CONTACT INFORMATION

Slavey Tanov
PhD Student
Div. Combustion Engines Dept. Energy Sciences, Lund University, Sweden
e-mail: slavey.tanov@energy.lth.se

ACKNOWLEGDEMENT

The author acknowledges the Competence Centre Combustion Processes (KCFP), Swedish Energy Agency Grant number 22485-2, for their financial support and to Dantec for the laser system and software.

The research leading to these results has received funding from the People Programme (Marie Curie Actions) of the European Union's Seventh Framework Programme FP7/2007-2013/ under REA grant agreement n° 607214.